

**Microstructural and compositional evolution of $\text{YBa}_2\text{Cu}_3\text{O}_{7.8}$ films grown by
MOCVD**

M. S. Hatzistergos ^a, H. Efstathiadis ^{a,*}, J. L. Reeves ^b, V. Selvamanickam ^b, L. P. Allen ^c,

E. Lifshin ^a and P. Haldar ^a

^a School of NanoSciences and NanoEngineering,
The University at Albany-SUNY, Albany, NY 12203

^b SuperPower Inc., Schenectady, New York, 12304

^c Epion Corporation, Billerica, MA, 01821

(To be submitted to the journal **PHYSICA C**)

PACS: 74.72.Bk; 74.76.Bz; 74.76.-w; 81.20.Fw; 85.25.Kx

Keywords: YBCO; Microstructure; MOCVD; FIB; SEM; EDS; XRD; Gas Cluster Ion Beam

* Corresponding author address: School of NanoSciences and NanoEngineering, University at Albany – State University of New York, 251 Fuller Road, Albany, NY 12203, USA. Tel.: (518) 437-8605; fax: (518) 437-8687. E-mail address: hefstathiadis@uamail.albany.edu (H. Efstathiadis)

ABSTRACT

The microstructural and compositional evolution of thick ($> 1 \mu\text{m}$) high temperature superconducting $\text{YBa}_2\text{Cu}_3\text{O}_{7-x}$ (YBCO) films grown on single crystal SrTiO_3 substrates by the Metal Organic Chemical Vapor Deposition (MOCVD) process was investigated by focused ion beam microscopy, scanning electron microscopy, energy dispersive x-ray spectroscopy, x-ray diffraction, and atomic force microscopy. This study showed that as the MOCVD YBCO film thickness increased above $0.5 \mu\text{m}$, defects such as second phase particles, pores, and misaligned grains preferentially nucleated and grew at the YBCO surface. A portion of this defective top layer was eliminated from all the samples using a gas cluster ion beam (GCIB) process that first removed material with a focused argon cluster beam. Next, an oxygen cluster beam was used to smooth the surface and re-oxygenate the YBCO. Comparing the critical current (I_c) measured before and after GCIB processing showed that the I_c remained the same, and even improved, when part of the defective top layer was removed. This microstructural and electromagnetic "dead layer" is believed to be responsible for the overall I_c decrease of MOCVD YBCO films thicker than $0.5 \mu\text{m}$.

INTRODUCTION

High temperature superconductors (HTS), such as $\text{YBa}_2\text{Cu}_3\text{O}_{7-x}$ (YBCO) are useful for their ability to carry large amounts of current in high magnetic fields and temperatures above liquid nitrogen with zero resistance. HTS conductors can be incorporated in numerous electric power devices, including transmission cables, motors, generators, and transformers. To use YBCO in these applications, the critical current (I_c) values at liquid nitrogen temperatures must be increased to several hundred Amperes in superconductor that is several hundred meters long.

The most direct way to increase I_c is to increase YBCO film thickness while maintaining constant critical current density (J_c) [1, 2]. However, it has been shown previously for pulsed laser deposited YBCO films that J_c drops rapidly with increasing YBCO film thickness [1-4]. For example, Foltyn et al. [4] found that even though a 2000 nm thick YBCO film deposited on buffered metal substrates carried a maximum I_c of 200 A, J_c decreased as film thickness increased from 2000 nm to 4700 nm. This result implied that additional YBCO layers did not contribute to the overall I_c . To confirm this, Foltyn et al. used an ion milling process (Ar monomer ions at 150 – 300 eV) to remove the top layers of a 3000 nm and 4700 nm thick YBCO films and examined the electrical performance of the remaining film. They found that the top layers of these originally thick films carried little or no current.

In this study, we will show the existence of the microstructural and electromagnetic “dead layer” at the surface of thick MOCVD YBCO films by direct observation of cross-sectional and plan-view images and I_c measurements before and after ion beam smoothing. X-ray diffraction data and Monte-Carlo simulations of compositional data will show that the dead layer is composed of non-superconducting second phase particles and misaligned (a-axis) grains that

cause the increase of surface roughness with increasing YBCO film thickness.

The smoothing technique used in this study, gas cluster ion beam (GCIB) processing, is different than the conventional ion milling process commonly used in preparing transmission electron microscopy samples. We used a dual gas species, dual-energy GCIB process. The dual gas species provide sufficient high energy argon clusters for coarse polishing and relatively low energy oxygen clusters for fine polishing and maintaining oxygen stoichiometry in the films.

EXPERIMENTAL PROCEDURES

YBCO films of different thickness (500, 900, 1300 and 2400 nm) were grown on single crystal SrTiO₃ (STO) substrates by the MOCVD process described in [5]. Using a 30 kV beam of Ga⁺ ions, a FEI 200 Focused Ion Beam (FIB) tool was used to prepare cross-sections in user-defined regions of interest. FIB was also used to directly observe the microstructural variation from the substrate/film interface up to the MOCVD YBCO surface and accurately measure the YBCO film thickness. Qualitative composition analysis of the films and the various defects seen on the film surface was carried out by a Thermo NORAN Vantage Energy Dispersive Spectroscopy (EDS) system incorporated into a LEO 1550 Scanning Electron Microscope (SEM). EDS spectra were collected using a stable 15 keV electron beam in the SEM and collecting x-rays for the same amount of time from discrete, separate locations on the YBCO film and on the defective regions. X-Ray Diffraction (XRD) analysis of the films was carried out by a Scintag XDS 2000 diffractometer. Surface roughness of the YBCO film before and after GCIB processing was measured using a Digital Instruments Nanoscope Dimension 3100 Atomic Force Microscope (AFM). I_c measurements were made using a standard 4 point probe method at 77K, self-field, on microbridges chemically etched on the YBCO film.

After microstructural and compositional investigation of the as-deposited films, the samples were mounted on 8" diameter silicon wafers for GCIB processing. The MOCVD YBCO films were smoothed in two steps. First, Ar clusters at a dose of 10^{16} ions/cm² were used to thin the superconductor layer by several hundred nanometers. The non-reactive nature and the high energy of the clusters (30 keV) formed an impact crater sufficient for material removal. In general, the higher the energy, the deeper the crater on the target surface; the higher the dose of

the gas clusters, the larger the etch depth [6]. Second, a lower energy (10 keV) oxygen gas cluster at a dose of 10^{16} ions/cm² was used for smoothing. This step was also found to be necessary to maintain the YBCO surface stoichiometry. Since oxygen gas clusters themselves are reactive, the oxygen deficiency caused by the Ar cluster bombardment was decreased. Because of the finite depth of the low energy craters in conjunction with the reactive gas species, this second step of the GCIB process resulted in improved smoothing of the YBCO surface while minimizing subsurface damage.

RESULTS AND DISCUSSION

Defects believed to be responsible for decreasing J_c with increasing MOCVD YBCO thickness were directly observed in a series of cross-sectional FIB images shown in Figure 1. The 500 nm thick YBCO film (Figure 1a) appears relatively dense and well-connected near the substrate/film interface, with large white "islands" located only at the surface of the superconductor. The structure of the 900 nm thick YBCO film (Figure 1b) contains different types of defects, such as grains that appear to be misaligned compared to the bulk of the film (denoted with a circle in the image). Additional defects such as pores (illustrated with the arrow) and particles with different contrast than the rest of the YBCO film (denoted with a rectangle) are also evident. Cross-sectional images of the 1300 nm (Figure 1c) and 2400 nm (Figure 1d) films show that the same defects are present in the top half of these thicker MOCVD films.

Representative plan-view FIB images of the thinnest and thickest YBCO film surface are shown in Figure 2. Pores and islands can be seen on the surface of the 500 nm thick film (Figure 2a). The dashed line in Figure 2a shows the exact location where the FIB cross-section shown in Figure 1a was made. In the case of the 2400 nm thick film (Figure 2b), plan-view imaging shows a very defective surface consisting of thin rectangular grains which are believed to be misoriented (possibly a-axis) grains as well as black particles which are probably second phase, non-superconducting, particles since their contrast is quite different from the YBCO film contrast.

To investigate the composition of the defects in the MOCVD YBCO films, qualitative EDS analysis was performed on the islands in the 500 nm film and on the dark particles on the surface of the 2400 nm thick film. Figure 3a shows the EDS spectra taken from an island and from the

500 nm YBCO film. Overlaying these two spectra illustrates that the islands are yttrium deficient with variation in the barium and copper content. Comparing the spectra that were collected from the film and the dark particles (Figure 3b), the black particles appear to have slightly more barium, while the intensity of the yttrium and low energy copper L-lines are significantly decreased. The exact composition of the black particles cannot be unambiguously identified from the EDS data. This compositional uncertainty is because the beam energies used to efficiently excite the x-rays in this energy range also caused an increase in the x-ray excitation volume, resulting in detection of signal from both the particle and the material below the particle.

The EDS data in Figure 3b was further investigated by doing Monte Carlo simulations [7-9] to predict how peak intensities in EDS spectra would vary due to the presence of different second-phase particles on the surface of a stoichiometric YBCO film. In Figure 3b, note that the copper K-line intensity (at ~8.05 keV) in the EDS spectrum from the black particle remained constant while the copper L-line intensity (at ~0.93 keV) decreased compared to the EDS spectrum of the YBCO film. This variation can be explained by the fact that the copper K-lines excited in the underlying YBCO are highly energetic and can travel through the ~250 nm thick black particles without being significantly absorbed, while the lower energy copper L-lines are strongly absorbed. Next, Monte Carlo simulations were performed on various combinations of yttrium-poor and copper-poor second phase particles – BaCuO_2 , $\text{Ba}_2\text{CuO}_{3.33}$, $\text{Ba}_2\text{Y}_2\text{O}_5$ and BaO_2 – on YBCO/STO to predict the composition of the black particles. When the BaCuO_2 , $\text{Ba}_2\text{CuO}_{3.33}$ or $\text{Ba}_2\text{Y}_2\text{O}_5$ phase were used, the resulting intensity ratios of the Y-L, Cu-K and L-lines did not match the experimental EDS data. By replacing the composition of the dark particles with BaO_2 , the intensity ratios that Monte Carlo simulations predicted matched the

experimentally measured intensities. Therefore, further analysis of the EDS data seems to indicate that the dark particles on the thick YBCO films are BaO₂.

XRD was used to further confirm the composition of the defects in the MOCVD YBCO films. Figure 4 shows two normal θ - 2θ XRD spectra from the same 500 nm and 2400 nm YBCO films that were qualitatively analyzed with the EDS. Most of the intense peaks that are present in the XRD spectra correspond to the (00L) planes of YBCO. The extra peaks at 24.4, 31.7 and 39.0 degrees that appear in the case of the thin film correspond to Ba₂Cu₃O_{5+x} and CuO. This XRD data is consistent with the EDS data which showed that the islands seen in the cross-sectional and plan-view FIB images of the 500 nm thick MOCVD YBCO film were yttrium deficient. In the case of the thickest film, the extra peaks at 23.3 and 47.6 degrees at the XRD spectra correspond to a-axis YBCO grains, which is consistent with our hypothesis regarding the identity of the rectangular shaped grains in the plan-view images. The inset in the graph shows the peak splitting at a 2θ location of 47.6, indicating the presence of three different phases, BaO₂, (100) YBCO grains, and Ba₂Y₂O₅. The extra peaks at, 32.9, 33.9 35.6, and 48.7 degrees in the XRD spectrum correspond to (103) YBCO, Ba₂Cu₃O_{5+x}, CuO, and BaO₂. The main difference between the XRD spectra of the thick and thin YBCO films is the presence of BaO₂ in the thick, but not in the thin, YBCO film. Therefore, this XRD data is consistent with the Monte-Carlo prediction from the EDS data that the dark particles on the surface of the 2400 nm thick MOCVD YBCO film are BaO₂.

The microstructural and compositional evolution was investigated by a plurality of techniques, FIB, EDS, and XRD, which all give corroborating evidence that the directly observed defective layer near the surface of MOCVD films consists of pores, a-axis YBCO

grains, and second phase particles that most likely correspond to islands containing $\text{Ba}_2\text{Cu}_3\text{O}_{5+x}$ and CuO in thin films with additional particles of BaO_2 in thicker films.

These microstructural imperfections form a defective layer in the superconductor which is believed to be responsible for the decrease of J_c with increasing YBCO film thickness as shown in Figure 5. The trend of decreasing J_c with increasing superconductor thickness is not unique to MOCVD YBCO films; J_c was also found to decrease exponentially with YBCO film thickness grown by pulsed laser deposited (PLD) [1, 4].

The origin of the microstructural defects such as pores, a-axis grains and second phase particles may be attributed to thermodynamic and/or kinetic causes. Researchers have reported that increasing YBCO film thickness causes an increase in the rate of thermal radiation. Moreover, the YBCO film's thermal conductivity decreases with increasing thickness [1, 10]. The combination of these two factors may cause the surface temperature of films thicker than 300 nm to be at a lower temperature by at least 30 to 40 °C when compared to the surface temperature of the first few nanometers of the deposited YBCO film. This surface cooling during film growth may thermodynamically favor the formation of second-phase particles on the film surface. Once these non-superconducting particles nucleate and start growing, associated porosity and misaligned grain growth may follow.

An additional factor leading to formation of a defective layer in thick YBCO films may be due to the growth kinetics of the YBCO grains themselves. YBCO grains grown on STO substrates can have their c -axes parallel to either [001] direction (c grains) or [100] direction (a grains). The higher growth rate of a grains compared to the c grains [11] may result in the domination of a grains as the film grows thicker. Since a grains carry 2% to 3% of the current that c grains can carry [12], the J_c of thick YBCO films drops.

To prove that the microstructurally defective surface layer of the MOCVD YBCO films was also electromagnetically “dead”, GCIB processing was used to remove a portion of the defects. The effectiveness of GCIB in removing the surface defects is illustrated in Figure 6a and 6b, where the surface of a 1300 nm thick film can be seen before and after the ion beam processing. The number of dark particles has been significantly decreased after GCIB processing and the surface looks much smoother. AFM was used to quantify the surface roughness before and after GCIB. The roughness of the as-deposited YBCO films increased from 45 nm to 170 nm as film thickness increased from 500 nm to 2400 nm. These results are consistent with the FIB and SEM results that showed more pores, second phase particles, and YBCO grain misalignment on the surface of thicker films. The 10 μm x 10 μm AFM images shown in Figure 7 (top row) illustrate that the surface of as-deposited YBCO films is quite rough with island-like grain morphology. The AFM images in Figure 7 (bottom row) illustrate that even though GCIB processing did not entirely remove the surface defects which cause surface roughness, it significantly smoothed the surface of all samples processed by 25-50%. The roughness of the GCIB smoothed YBCO films was decreased from the original surface roughness and measured 10 nm and 100 nm for the thinnest and thickest YBCO films

The critical current (I_c) of the samples after GCIB processing was measured to be the same or even higher than the I_c of the samples before GCIB processing [3], indicating that the top defective layer seen in the FIB cross-sectional images did not carry much, if any, current. As a result, J_c increased by 35% to 85% due to GCIB removal of the defective layer. Unexpectedly, in the case of the 1300 and 2400 nm thick films, the I_c of the microbridge increased after GCIB processing from 4.4 A to 5.5 A and from 8.5 A to 11 A respectively. This I_c increase could be explained from the possibility that not all of the Ar and/or O₂ monomers were filtered out of the

beam. The greater penetration depth of the monomers may create flux pinning sites, which may explain the increase in I_c [13].

Further experiments are in progress to study the effect of GCIB processing on MOCVD YBCO coated conductors. The morphological and compositional evolution of YBCO films on buffered metal substrates will be compared with these single crystal substrate results. In addition, the GCIB processing conditions will be optimized in order to remove the dead layer before depositing additional YBCO layers to produce a coated conductor with thick YBCO and higher I_c than produced with a single layer.

CONCLUSIONS

As MOCVD YBCO grows thicker on single crystal STO substrates, microstructural defects start forming and thus degrade the current carrying performance of the superconductor. These defects were directly observed by FIB cross-sectional and plan-view imaging and their composition was determined through XRD, EDS and Monte Carlo simulations. After GCIB processing removed the top ~30% of the film that contained pores, a-axis YBCO grains and second phase particles, the current carrying capability of the samples remained the same or improved. This indicates that the microstructurally defective surface layer of thick MOCVD YBCO films was an electromagnetically dead layer.

ACKNOWLEDGMENTS

This research was supported in part by the U.S. Air Force Office of Scientific Research and Albany NanoTech at the University at Albany – SUNY. The work of R. MacCrimmon, C. Santeufemio and A. Cate at Epion and L. Hope, G. Carota, M. Funk, and H.G. Lee at SuperPower is greatly appreciated.

REFERENCES

- [1] B. W. Kang, A. Goyal, D. F. Lee, J. E. Mahtis, E. D. Specht, P. M. Martin, D. M. Kroeger, M. Paranthaman and S.Sathyamurthy, *J. Mater. Res.* **17**, 1750 (2002).
- [2] Q. X. Jia, S. R. Foltyn, P. N. Arendt, and J. F. Smith, *Appl. Phys. Lett.* **80**, 1601 (2002).
- [3] M. S. Hatzistergos, H. Efstathiadis, E. Lifshin, A. E. Kaloyeros, J. L. Reeves, V. Selvamanickam, L. P. Allen and R. MacCrimmon, *IEEE Trans Appl. Super* **13**, 2470-2473 (2003).
- [4] S. R. Foltyn, Q. X. Jia, P. N. Arendt, L. Kinder, Y. Fan, and J. F. Smith, *Appl. Phys. Lett.* **75**, 3692 (1999).
- [5] V. Selvananickam, G. B. Galinski, G. Carota, J. DeFrank, C. Trautwein, P. Haldar, U. Balachandran, M. Chudzik, J. Y. Coulter, P. N. Arendt, J. R. Groves, R. F. DePaula, B. E. Newman, and D. E. Peterson, *Physica C* **333**, 155-162 (2000).
- [6] L. P. Allen, Z. Insepov, D. B. Fenner, C. Santeufemio, W. Brooks, K. S. Jones and I. Yamada, *J. Appl. Phys.* **92**, 3671 (2002).
- [7] Berger, M. (1963). *Methods in Computational Physics I*. Academic, New York.
- [8] Shimizu R., and K. Murata, *J. Appl. Phys. Lett.* **42**, 387 (1971).
- [9] Heinrich, K. F. J., and D. E. Newbury, eds. (1991). *Electron Probe Quantification*. Plenum, New York.
- [10] Moreno, F. Garcia (1995). *Diplomarbeit*, University of Göttingen, Göttingen, Germany.
- [11] C. W. Nieh, L. Anthony, J. Y. Josefowicz and F. G. Krajenbrink, *Appl. Phys. Lett.* **56**, 21 (1990).
- [12] S. R. Foltyn, P. Tiwari, R. C. Dye, M. Q. Le and X. D. Wu, *Appl. Phys. Lett.* **63**, 13 (1993).

- [13] A. Ignatiev, Q. Zhong, P. C. Chou, X. Zhang, J. R. Liu and W. K. Chu, *Appl. Phys. Lett.* **70**, 1474 (1997).

FIGURE CAPTIONS

Figure 1. FIB cross-sectional images (tilted by 45°) of superconductor films on STO substrates with different YBCO thickness values: (a) 500 nm (b) 900 nm, (c) 1300 nm, and (d) 2400 nm. The pores (denoted by an arrow), misoriented YBCO grains (in circled regions), and second phase particles (in rectangular regions) comprise a defective layer near the surface of the YBCO films.

Figure 2. Plan-view FIB images of the (a) 500 nm and (b) 2400 nm thick YBCO films showing the different defects on the surface of the thin and thick superconducting films. Pores and islands dominate the microstructure of the 500 nm film, with a-axis grains and second phase particles on the surface of the 2400 nm film.

Figure 3. Comparison of the EDS spectra from the (a) islands and film of the 500 nm thick sample and (b) black particles and film of the 2400 nm thick sample. Qualitative EDS analysis shows that the islands are yttrium deficient and the black particles are barium rich.

Figure 4. A comparison of the normal XRD θ - 2θ scans from the 500 nm and 2400 nm YBCO films. $\text{Ba}_2\text{Cu}_3\text{O}_{5+x}$ and CuO are second phase particles comprising the islands in the thin film, with additional BaO_2 in the thick film.

Figure 5. Critical current density versus superconductor thickness for MOCVD and PLD YBCO films. A decrease in J_c with increasing YBCO thickness is observed.

Figure 6. Plan-view FIB images of the 1300 nm sample (a) before and (b) after GCIB processing. The images show that GCIB was effective at smoothing the films by removing defects, such as the black second phase particles, from the surface.

Figure 7. Comparison of YBCO film roughness before and after GCIB processing. AFM images of the (a) 500 nm, (b) 900 nm, (c) 1300 nm, and (d) 2400 nm thick YBCO films before smoothing showing increasing surface roughness with increasing film thickness. AFM images of these same films after smoothing (e), (f), (g), and (h) show the effectiveness of GCIB smoothing. All AFM scans were $10\ \mu\text{m} \times 10\ \mu\text{m}$ in size and the z-axis interval was $1\ \mu\text{m}$.

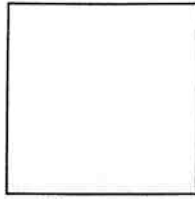
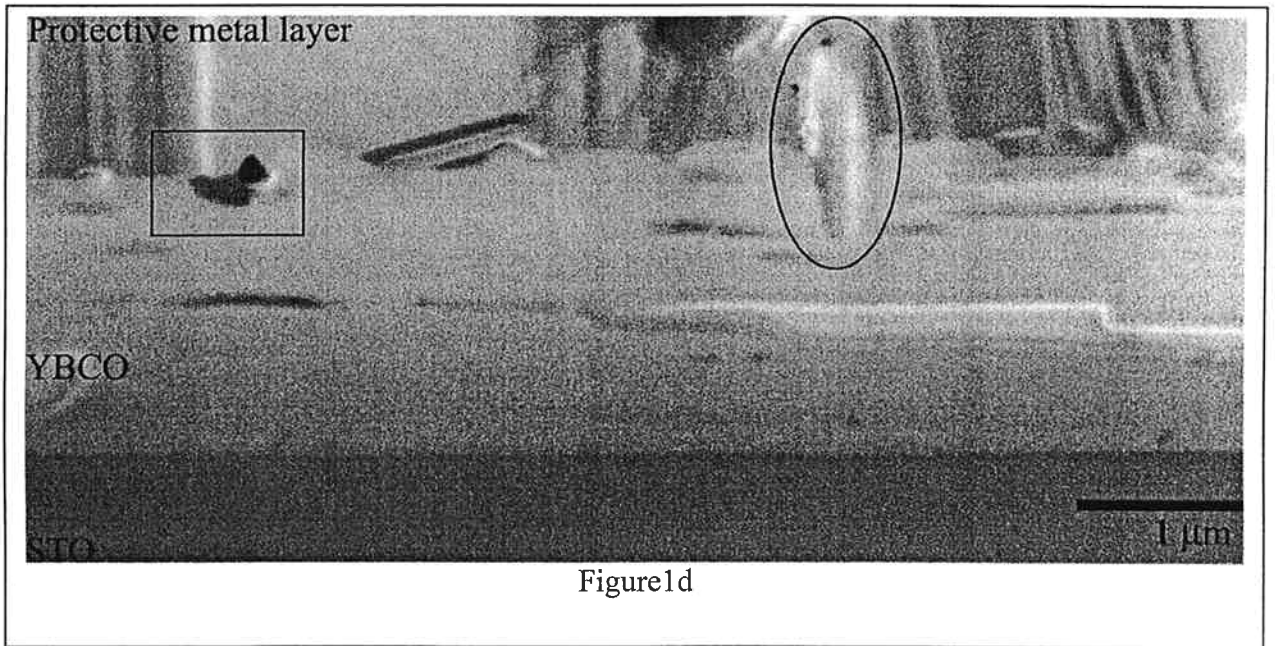
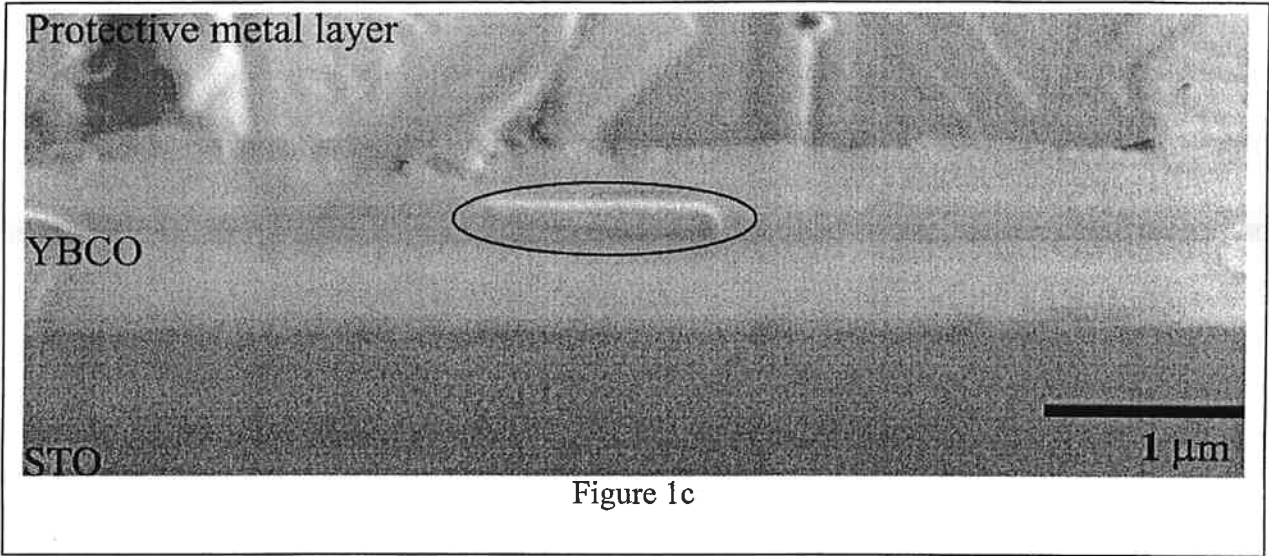


Figure 1a



Figure 1b



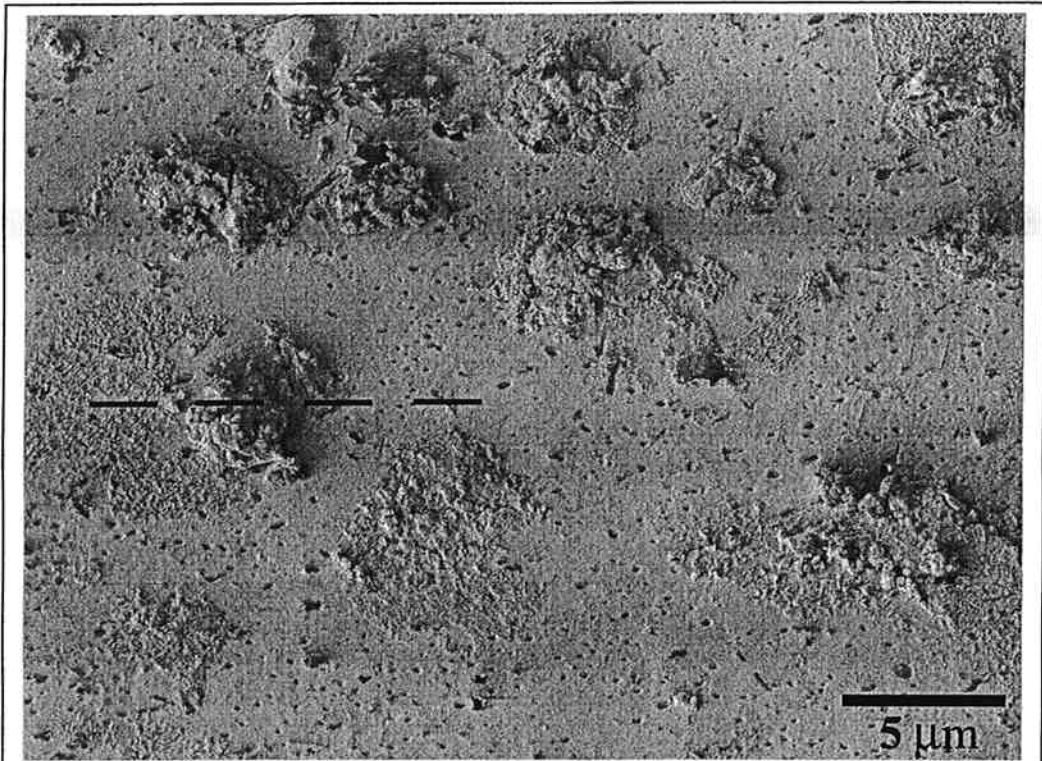


Figure 2a



Figure 2b

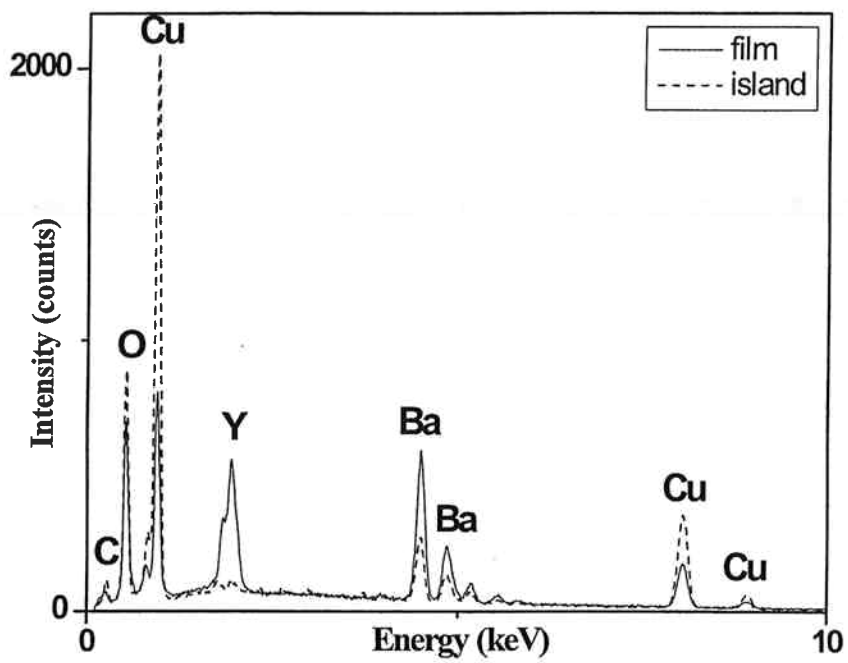


Figure 3a

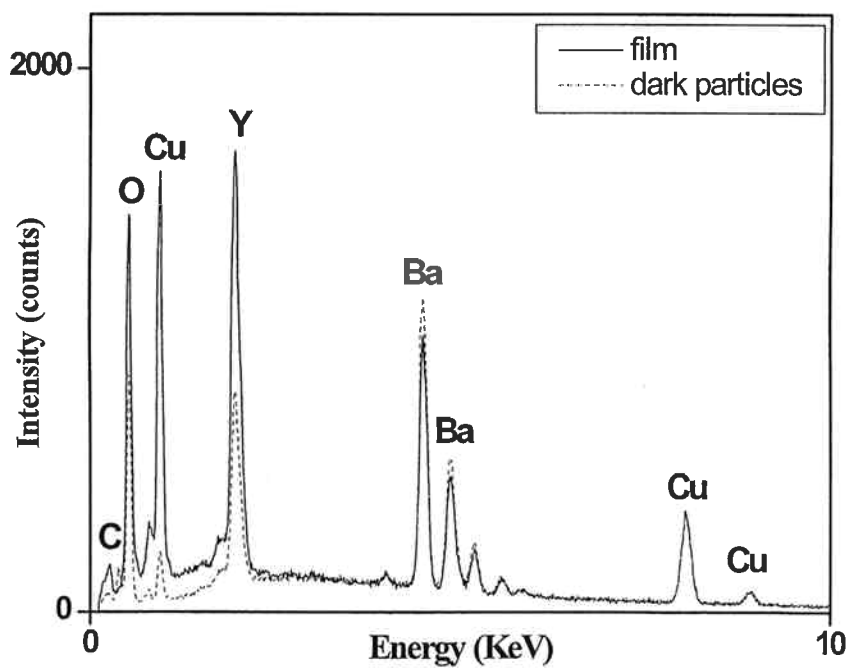


Figure 3b

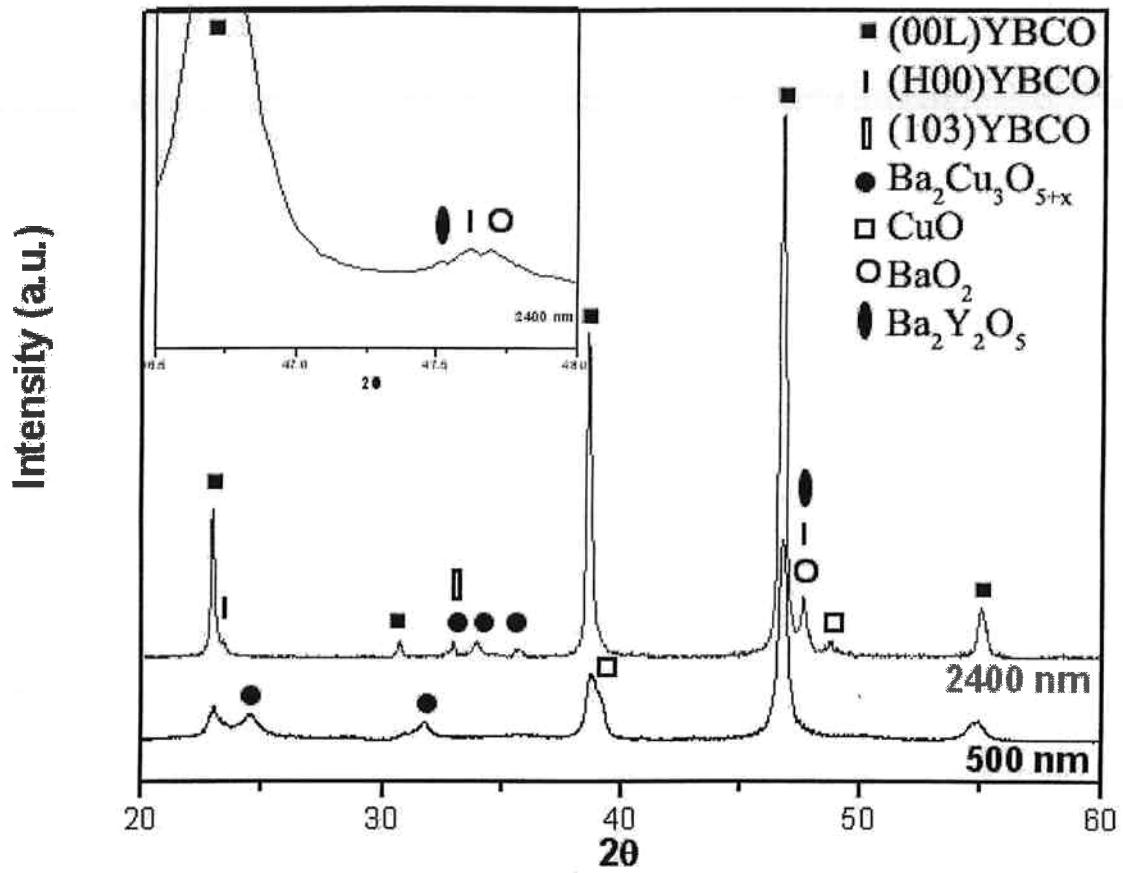


Figure 4

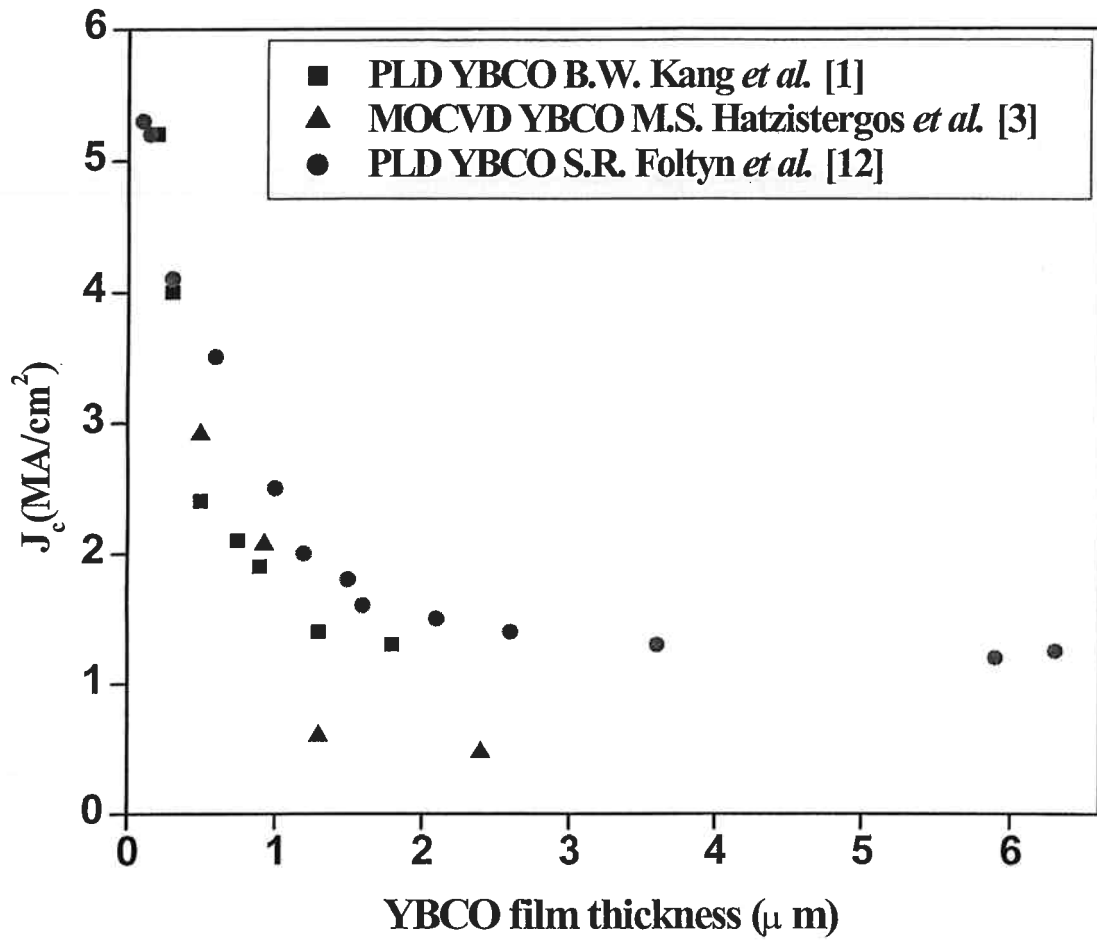


Figure 5

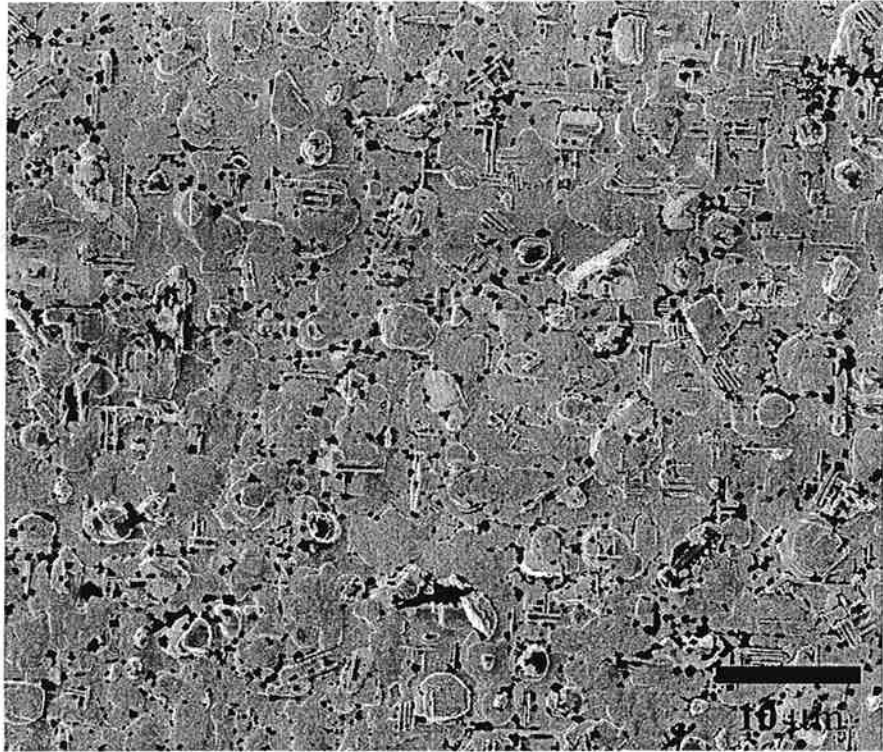


Figure 6a

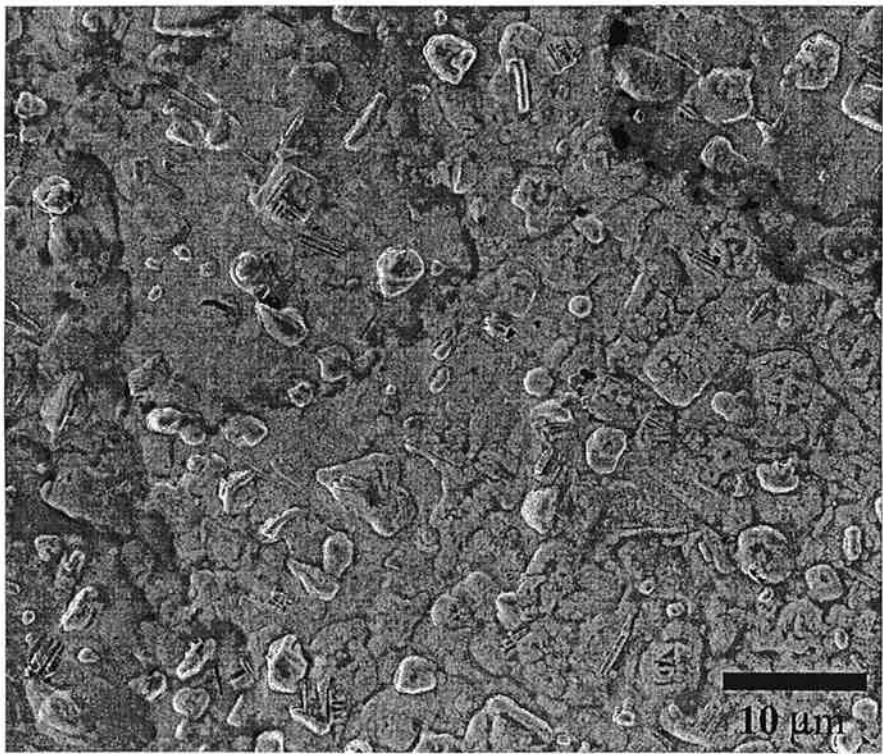


Figure 6b

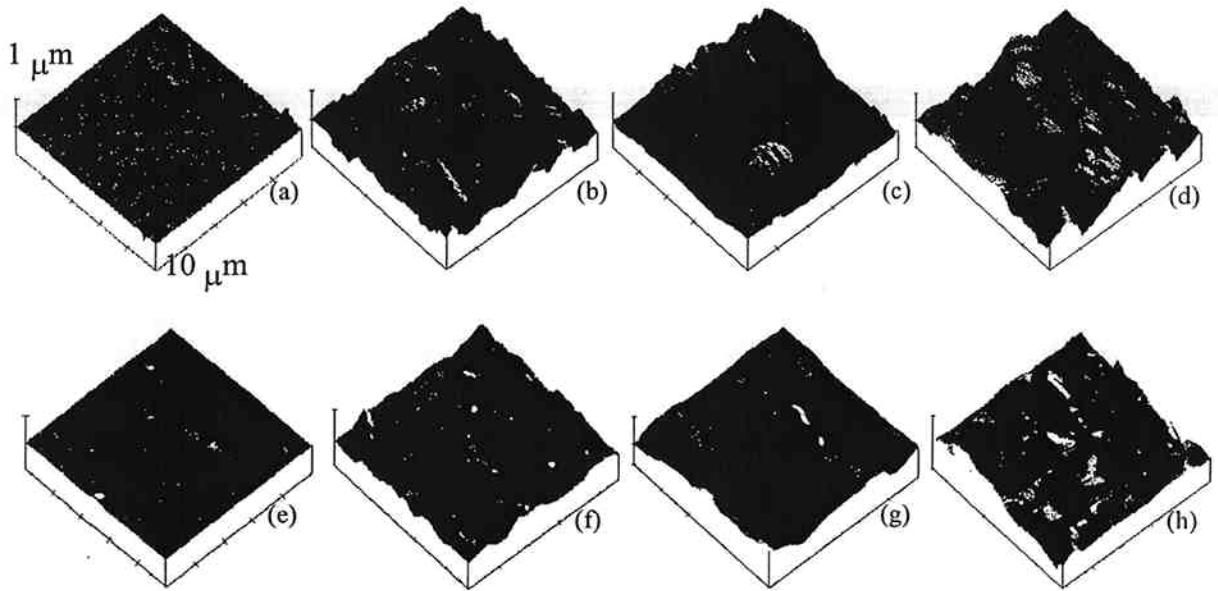


Figure 7